Plant leaf identification based on volumetric fractal dimension

Andre Ricardo Backes Dalcimar Casanova Odemir Martinez Bruno

July 29, 2008

Abstract

Texture is an important visual attribute used to describe the pixel organization in an image. As well as it being easily identified by humans, its analysis process demands a high level of sophistication and computer complexity. This paper presents a novel approach for texture analysis, based on the analysis of the complexity of the surface generated from a texture, in order to describe and characterize it. The proposed method produces a texture signature which is able to efficiently characterize different texture classes. The paper also illustrates a novel method performance on an experiment using texture images of leaves. Leaf identification is a difficult and complex task due to the nature of plants, which presents a huge pattern variation. The high classification rate yielded shows the potential of the method, improving on traditional texture techniques, such as Gabor filters and Fourier analysis.

1 Introduction

Plant identification has an important role in current scientific problems such as biodiversity, ecology and pharmacology among others. In Biology, plant identification involves analysing many organs, such as flowers, seeds, leaves and woody parts [18, 20]. This approach renders the task difficult as flowers and seeds, which are seasonal and dependent on the plant's age and environment, are not easy to find. In special situations such as finding fossils or rare plants, the material available to identify a plant is just the leaves. In order to solve these situations, a leaf morphological taxonomy technique is proposed, which considers only the leaves to perform the identification tasks [14]. This approach combines various features of leaves such as shape, vein structure, texture and also some histological information.

Identifying plants is a difficult and complex task due to the nature of the leaves. Although the leaves present some fundamental features, they also present a wide pattern variation. This variation may occur in different leaves from the same plant, where characteristics such as maturity and exposure to the sun produces variations in the size, color, texture and shape of the leaves. These variations are also present in leaves from the same species, but from different plants. In this case, they are a consequence of soil influence, climate or even environment when the leaf is being formed.

In computer vision literature, the few approaches found use contour-based and geometry features for leaf classification [21, 11, 30, 32]. This work presents a novel approach to identify plants based on the texture/complexity of their leaves. A novel methodology based on the volumetric fractal dimension is proposed, which extracts features from the images of the leaves providing information to identify them.

Over the years, researchers have studied features for texture analysis. Many of these fea-

tures represent the local behavior of the texture via the second-order statistics [13, 24]. Recently, texture features representing subbands to provide a compact description of the harmonics in the texture using Gabor transforms [28, 4, 16, 10, 23], Fourier analysis [1, 2] and wavelet packets [27, 31], have been used to provide a compact description of the harmonics in the texture. However, these methods fail to distinguish many natural textures that show no periodic structure [15, 19]. Natural textures may not present any detectable quasi-periodic structure. Instead, they show random but persistent patterns that result in a cloud like texture appearance. Examples of these "*cloudy*" textures are widely found on the surface of plant leaves.

Fractals offer an alternative to these approaches, as these objects represent shape and natural phenomena. Fractal surfaces can be considered as those surfaces of which the topological dimension takes non-integer values (non-Euclidean geometry). Most of the natural surfaces, such as coastlines, brick, skin, rocks, etc., can be modeled as fractal surfaces. Therefore, the classification problem is reduced to estimating the fractal dimension of the object. As the fractal feature is an inherent property of the region/surface/object, it can be a more reliable measure. The proposed method generates a surface in R^3 as a representation of a texture image in R^2. Consequently, the complexity analysis is done by applying the Bouligand-Minkowski fractal dimension method [26, 29] to the calculated surface. Our main interest is to achieve a signature from the calculated influence volume of the surface.

This paper is organized as follows: Section 2 presents the volumetric fractal dimension technique, Section 3 shows the proposed texture signature and illustrates how to perform texture feature extraction using volumetric fractal dimension, in Section 4 we describe how the leaf database was composed, Section 5 presents the experiments and results and Section 6 concludes this paper.

2 Volumetric fractal dimension

Complexity is a term largely used in the literature, but, in spite of its importance, it lacks an exact definition. It can be understood as a measure of how irregular an object is. The literature presents various ways of estimating the complexity of an object, and an interesting way is to estimate the fractal dimension of this object [8, 11, 22, 9, 7].

Fractal dimension describes how irregular an object is. Unlike topological dimension, which is an integer value which describes the number of dimensions where an object is inserted, fractal dimension is a fractionary value which describes how much of the space an object occupies [11, 22, 9, 26, 29].

One of the most accurate methods to compute the fractal dimension is the Bouligand-Minkowski [29, 11, 6]. It is based on the study of the influence area, $A(r)$, created by the dilatation of image A by a disc of radius r. This influence area $A(r)$ is very sensitive to structural changes of the object, and consequently, even small changes in the object can be detected. The Bouligand-Minkowski fractal dimension, FD, is defined as:

$$FD = N - \lim_{r \to 0} \frac{\log A(r)}{\log r}$$

with

$$A(r) = \left\{ p' \in R^N | \exists p \in A : \left| p - p' \right| \leq r \right\},$$

where p is a point from image A, p' is a point in R^N whose distance form p is smaller or equal to r and N is the number of dimensions of the space where image A is inserted. For binary images, $N = 2$.

In order to compute the Bouligand-Minkowski fractal dimension of a gray-scale image, the following approach is proposed. Given a gray-scale image $A \in R^2$, a surface $S \in R^3$ is generated. This surface is generated transforming each image pixel into a point $p = (y, x, z)$, $p \in S$, where y and x correspond to the coordinates of the pixel in image A and $z = A(y, x)$ is its intensity. Figure 1 shows this process.

By performing the dilatation of surface S by a radius r, the Bouligand-Minkowski fractal dimension FD of S can be estimated:

$$FD = 3 - \lim_{r \to 0} \frac{\log V(r)}{\log (r)}$$

with

$$V(r) = \left\{ p' \in R^3 | \exists p \in S : \left| p - p' \right| \leq r \right\},$$

where $p' = (x', y', z')$ is a point in R^3 whose distance form $p = (x, y, z)$ is smaller or equal to r and $V(r)$ is the influence volume calculated by dilating each point of S by a sphere of radius r. Figure 2 shows an example of fractal dimension computed for different texture images.

3 Proposed texture signature

Tables 1 and 2 show the distance maps computed from binary images after the dilation process takes place. Each table presents two points marked with a zero value. These are points of interest in the image. Remaining points represent the influence area $A(r)$ and the value assigned represents the minimum distance from that point to a point marked with zero. The influence area $A(r)$ for a given radius r is the number of points in the distance map whose values are equal or smaller than r.

Note that according to the disposition of the interest point in the image, the dilatation process changes. Thereby, the influence area also changes. This makes the method very sensitive to structural changes in the image, as seen when the values of the influence area for both tables are compared. This difference between values increases according to the image structure, and also as the radius increases.

This behavior pattern also occurs in gray-scale images. As the r value increases, the spheres produced by different points of surface S start to interact with each other. This interaction among different spheres disturbs the way the influence volume $V(r)$ increases, and it can detect even small changes in the texture. An example of this dilation process in texture images can be seen in Figure 3.

Different textures have different pixel organization. This reflects a characteristic pattern for specific textures. Each pattern produces an influence volume characteristic for a specific kind of texture. This makes it possible to use $V(r)$ as a texture feature which describes the way that different pixels are organized on the texture and, consequently, the complexity of the texture.

In this paper, we propose the use of the influence volume $V(r)$ as a feasible signature technique, which conveys the complexity of the pixel organization of the image and, therefore, is capable of representing or characterizing texture by a function or a feature vector [11]. As $V(r)$ describes the texture organization for a specific radius r, we propose a novel texture signature $\psi(r_{max})$. This signature consists of the concatenation of the logarithm of the influence volume, $V(r)$, calculated for all values of $r \in E$, where E is the set of sorted Euclidean distances for a given maximum radius r_{max}:

$$E = \left\{ 1, \sqrt{2}, \sqrt{3}, \ldots, r_{max} \right\},$$

$$\psi(r_{max}) = \Big[\log V(1), \log V(\sqrt{2}), \log V(\sqrt{3}), \ldots, \log V(r_{max}) \Big]$$

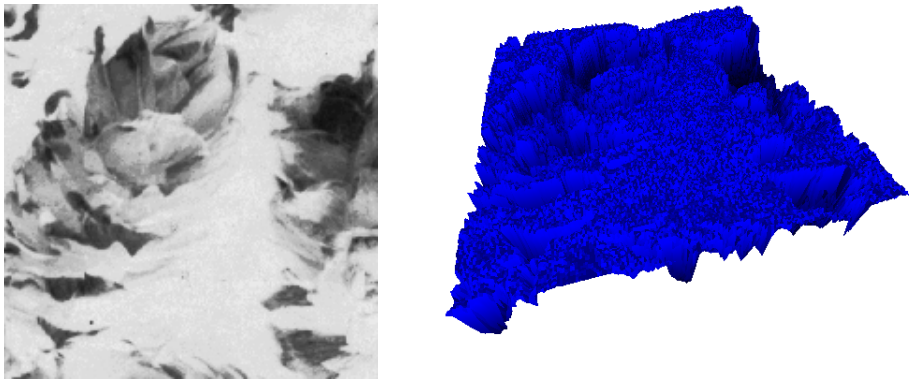

(a) (b)

Figure 1: Surface generated from an image texture: (a) original texture; (b) surface.

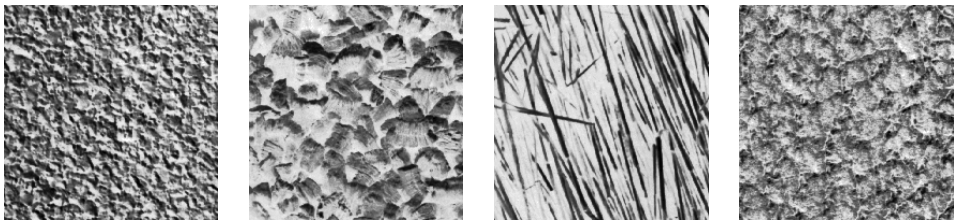

$FD = 2.2169$ $FD = 2.1289$ $FD = 2.1382$ $FD = 2.1715$

Figure 2: Bouligand-Minkowski fractal dimension for different texture images when $r = 20$ is considered.

$\sqrt{18}$	$\sqrt{13}$	$\sqrt{10}$	3	$\sqrt{10}$	$\sqrt{13}$	$\sqrt{18}$	5
$\sqrt{13}$	$\sqrt{8}$	$\sqrt{5}$	2	$\sqrt{5}$	$\sqrt{8}$	$\sqrt{13}$	$\sqrt{20}$
$\sqrt{10}$	$\sqrt{5}$	$\sqrt{2}$	1	$\sqrt{2}$	$\sqrt{5}$	$\sqrt{10}$	$\sqrt{17}$
3	2	1	0	1	2	$\sqrt{8}$	$\sqrt{13}$
$\sqrt{10}$	$\sqrt{5}$	$\sqrt{2}$	1	1	$\sqrt{2}$	$\sqrt{5}$	$\sqrt{10}$
$\sqrt{13}$	$\sqrt{8}$	2	1	0	1	2	3
$\sqrt{17}$	$\sqrt{10}$	$\sqrt{5}$	$\sqrt{2}$	1	$\sqrt{2}$	$\sqrt{5}$	$\sqrt{10}$
$\sqrt{20}$	$\sqrt{13}$	$\sqrt{8}$	$\sqrt{5}$	2	$\sqrt{5}$	$\sqrt{8}$	$\sqrt{13}$

Table 1: Example of influence area calculation for a binary image. Cells marked with zero correspond to points of the image. The value of some influence area $A(r)$ according to radius r: $A(0) = 2$; $A(1) = 10$; $A(\sqrt{2}) = 16$; $A(2) = 22$; $A(\sqrt{5}) = 32$.

Note that the $V(r)$ value when $r = 0$ is not considered in the signature. This value corresponds to the surface of the image. In fact, for an experiment using images of equal size, this value has no relevance.

The use of different r values enables us to study the texture complexity at different scales. It performs a better discrimination and classification of the texture, as the micro and macro texture information is considered.

$\sqrt{18}$	$\sqrt{13}$	$\sqrt{10}$	3	$\sqrt{10}$	$\sqrt{13}$	$\sqrt{18}$	5
$\sqrt{13}$	$\sqrt{8}$	$\sqrt{5}$	2	$\sqrt{5}$	$\sqrt{8}$	$\sqrt{13}$	$\sqrt{18}$
$\sqrt{10}$	$\sqrt{5}$	$\sqrt{2}$	1	$\sqrt{2}$	$\sqrt{5}$	$\sqrt{8}$	$\sqrt{13}$
3	2	1	0	1	$\sqrt{2}$	$\sqrt{5}$	$\sqrt{10}$
$\sqrt{10}$	$\sqrt{5}$	$\sqrt{2}$	1	0	1	2	3
$\sqrt{13}$	$\sqrt{8}$	$\sqrt{5}$	$\sqrt{2}$	1	$\sqrt{2}$	$\sqrt{5}$	$\sqrt{10}$
$\sqrt{18}$	$\sqrt{13}$	$\sqrt{8}$	$\sqrt{5}$	2	$\sqrt{5}$	$\sqrt{8}$	$\sqrt{13}$
5	$\sqrt{18}$	$\sqrt{13}$	$\sqrt{10}$	3	$\sqrt{10}$	$\sqrt{13}$	$\sqrt{18}$

Table 2: Example of influence area calculation for a binary image. Cells marked with zero correspond to points of the image. Value of some influence area $A(r)$ according to radius r: $A(0) = 2$; $A(1) = 8$; $A(\sqrt{2}) = 14$; $A(2) = 18$; $A(\sqrt{5}) = 28$.

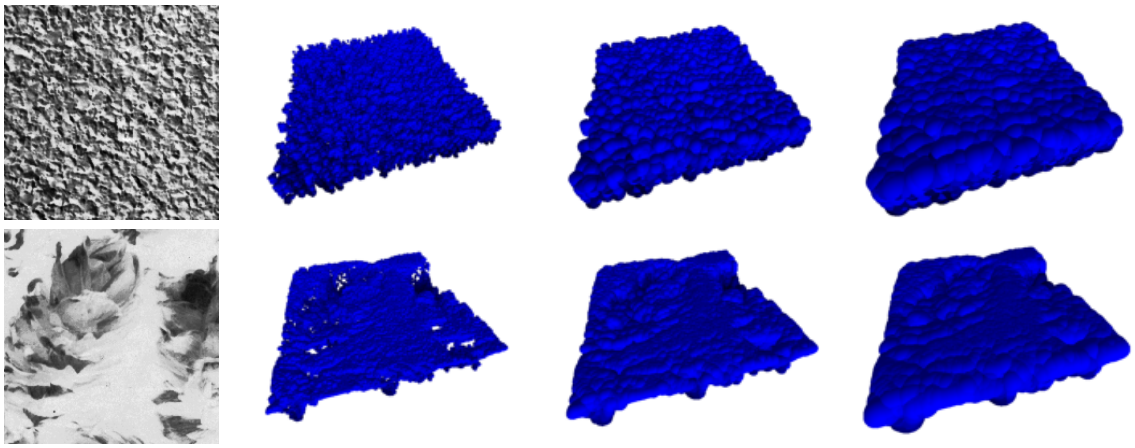

(a) (b) (c) (d)

Figure 3: Influence volume characteristic for specific texture pattern: (a) original texture; (b) $r = 2$; (c) $r = 5$; (d) $r = 10$.

Moreover, this approach makes it add a larger quantity of information concerning texture behavior for the proposed texture signature vector using a small number of descriptors.

Figure 4 shows an example of signatures computed for the textures shown in Figure 2. Initially, the spheres can dilate freely, without interacting with each other. As a result, we note similar behavior at a small radius for different texture classes. Otherwise, as the radius increases, the spheres start to intercept with each other, i.e., the volume of the spheres is shared among two or more spheres and the surface volume is no longer the sum of the volume of each individual sphere. This changes the way the surface volume increases, showing the differences among various texture classes and thus making it possible to identify them.

4 Leaf Database

In order to carry out the experiments, a database with 400 leaves from Brazilian flora, divided into 10 classes, was manually collected *in vivo*, and each leaf was washed to remove impurities, adjusted to its central axis a (line that

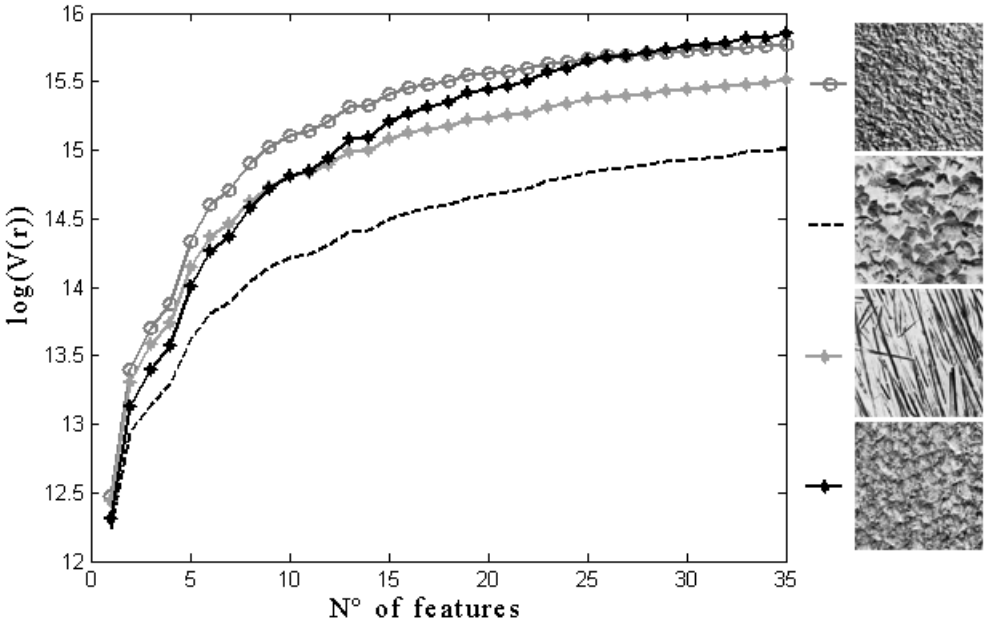

Figure 4: Proposed signature computed for the textures shown in Figure 2

connects the basal and apical ends) to stand in a vertical position, and digitalized by a scanner using a 1200dpi *(dots per inch)* resolution. Figure 5 shows a texture from each plant species and Figure 6 shows a texture found in each species. A *lossless* compression was used to store the images without information loss.

In order to do the proposed experiment a texture sample from the digitalized leaves (Texture Windows) had to be extracted. Each texture window has 128×128 pixels of size. This task was performed by an automatic algorithm, which extracts, without overlapping, 30 texture windows from each leaf. Figure 7 illustrates this process as well as 3 texture windows.

However, due to the great variability of textures presented in a single leaf (Figure 8) and the need of texture examples without noise (fungus, plague, injuries, etc) and great color variance or structural information (skeleton), it is necessary to choose a total of W windows which better describe the texture under analysis. A simple approach to perform this task is to use the mean and variance of each quadrant of the texture window to compose a feature vector $\mathbf{x}$ and, using a distance metric, to discard the texture windows whose feature vector presents the highest difference when compared to the mean of its class/specie (outliers). Considering $q_{ik}(x,y), i = 1 \ldots 4$, quadrants of a texture window $f_i(x,y)$ the corresponding feature vector $\mathbf{x}_i$ is computed in the following way:

$$\mathbf{x}_i = \mu_{q_{i1}}, \sigma_{q_{i1}}, \mu_{q_{i2}}, \sigma_{q_{i2}}, \ldots, \mu_{q_{i4}}, \sigma_{q_{i4}}$$

where

$$\mu_{q_{ik}} = \frac{1}{mn} \sum_{x=1,y=1}^{m,n} q_{ik}(x,y)$$

and

$$\sigma^2_{q_{ik}=} = \frac{1}{mn} \sum_{x=1,y=1}^{N} (q_{ik}(x,y) - \mu)^2$$

Figure 5: Leaves collected *in vivo* and digitalized at 1200dpi resolution.

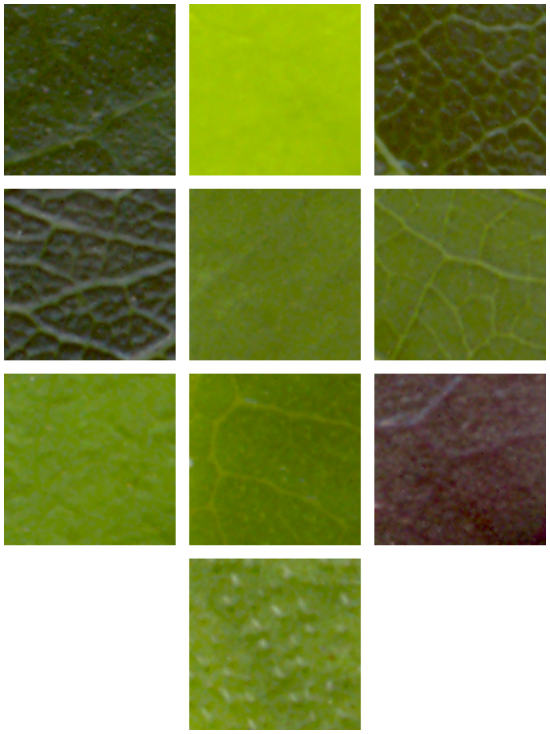

Figure 6: Example of a texture for each collected plant species.

According to Barnett and Lewis [3], the outlier identification in multivariate data is usually performed using the principle of *reduced subordering*. This method transforms a multivariate observation $\mathbf{x}$, of p dimensions, into a scalar $R(\mathbf{x})$. Therefore, the samples $\mathbf{x}_1, \mathbf{x}_2, \ldots, \mathbf{x}_n$ can be sorted according to the values of $R_j = R(\mathbf{x}_j)(j = 1, 2, \ldots, n)$ and observation $\mathbf{x}_i$ with the highest value for R_n is a candidate to be an outlier. A technique widely used is to represent a multivariate observation $\mathbf{x}$ by a distance metric. Considering that the values that compose the $\mathbf{x}$ are dependent, we can use the Mahalanobis distance:

$$R(\mathbf{x}; \mathbf{x}_0) = \sqrt{(\mathbf{x} - \mathbf{x}_0)^T \Sigma^{-1} (\mathbf{x} - \mathbf{x}_0)}$$

where Σ is the covariance matrix and $\mathbf{x}_0$ reflects the implied data localization or distribution. For a normal data distribution, it is common to use the real mean μ as the referential point $\mathbf{x}_0$.

The scalar value R_i denotes the similarity degree between pattern $\mathbf{x}_i$ and the mean μ. Observation $\mathbf{x}_i$ with the highest value R_n is discarded as being an outlier. Next, the mean μ and the R_i distances of the remaining observations are recomputed and a new outlier is eliminated. This discarding process is carried out until a set of W which is the most similar is obtained and representative observations in the database remain. Figure 8 shows 25 dis-

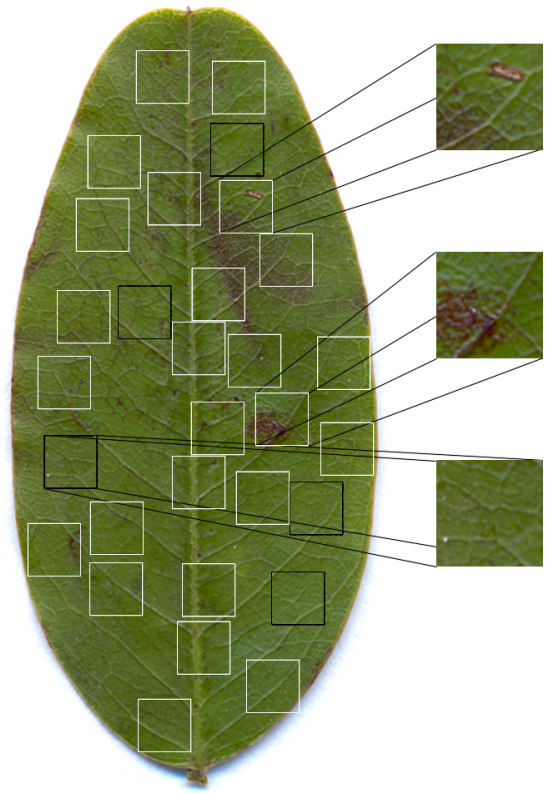

Figure 7: Texture windows extracted from a leaf: in white, discarded windows; in black, texture windows used in the experiment.

carded texture windows (outliers) and 5 windows remaining for a given leaf sample. Figure 7 shows (in black) the location of the 5 texture windows selected. We note the method is able to choose, among the original set of windows, the most meaningful windows, without noise or structural information.

5 Evaluation

For each leaf sample previously considered, 5 texture windows are extracted. Therefore, a database with 2,000 texture windows (or samples), divided into 10 classes, is compiled.

The proposed texture signature is applied over each texture window selected. Each sample is characterized by p features (where p depends on the r_{max} considered) and the classes are known *a priori*. Therefore, we can evaluate the quality of the method using statistical analysis, like linear discriminant analysis [12, 25]. Let $f_i(\mathbf{x})$ be the density function of the population $i, i = 1, 2, \ldots, g$, the probability of misclassification is minimized according to the following discrimination rule: for a fix observation $\mathbf{x}$, compute the density value $f_i(\mathbf{x})$ for each population $i, i = 1, 2, \ldots, g$, and classify the observation in population k which presents the highest $f_i(\mathbf{x})$ value, i.e.:

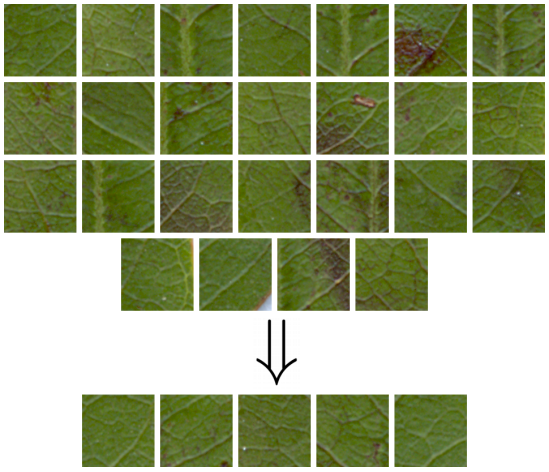

Figure 8: Top: texture windows discarded (outliers). Down: texture windows selected.

$$f_k(\mathbf{x}) = \arg\max\{f_i(\mathbf{x}), i = 1, 2, \ldots, g\}$$

with

$$f_i(\mathbf{x}) = -\frac{1}{2}\ln(|\Sigma_i|) - \frac{1}{2}(x - \mu_i)'\Sigma_i^{-1}(x - \mu_i))$$

where μ and Σ_i are, respectively, the average vector and covariance matrix of the population $i, i = 1, 2, \ldots, g$. In Johnson and Wichern [17], more details are presented concerning the mathematical formulation of the discriminant function.

Moreover, we use 1200 samples for training and the remaining 800 samples for testing. The 1200 samples are selected randomly from all 2000 samples, ensuring there are 3 samples of each class. This training and testing scenario is repeated 10 times to compute the average number of correctly classified samples and the variance.

The average classification accuracies (percentage correct), variance, number of features, reliability (average *a posteriori* probability for samples correctly classified) and maximum errors are presented for a specific class in Table 3. Different r_{max} values are considered as a way to evaluate the influence of this parameter in the final results.

Note that, as the radius increases, more information about the texture in different scales is added to the signature vector, improving the success rate. The misclassification rate per class also decreases, i.e., the computed descriptors can discriminate different classes with considerable quality. However, after some specific radius, the information added to the signature vector is no longer relevant (e.g. success rates for $r_{max} = 9 \approx r_{max} = 16$), causing misclassification of the samples. However, this misclassification is minimum and does not affect the performance of the method.

Figure 9 illustrates this misclassification. Note that, the misclassification observed in the experiment is due to similar influence volumes obtained for different textures. After a specific radius, the dilated spheres become so big for a texture pattern, that all relevant information about this pattern is already incorporated into the influence volume. This new information does not represent the pixel interaction in the texture, but the tendency of the Fractal Dimension to converge to zero. This zero tendency is common for all texture patterns and it acts as a noise in the classification process, decreasing the success rate.

Table 4 shows the confusion matrix achieved

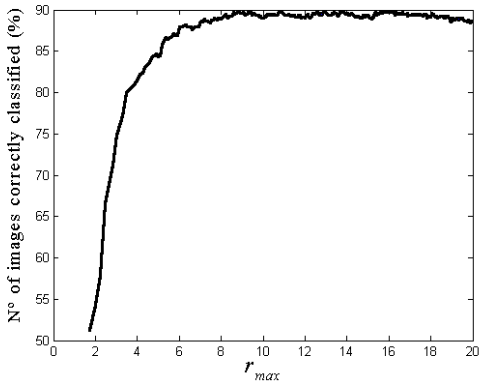

Figure 9: N^o of images correctly classified against maximum dilatation radius r_{max}.

for $r_{max} = 9$ while Table 5 summarizes the *posteriori* probabilities for each class (results for a unique training and testing scenario). This information shows that classes C01 and C07 present more outliers (higher misclassification), and they are the classes which are most difficult to recognize because their *posteriori* probability (reliability of a sample to be classified correctly) is the lowest among all classes. On the other hand, class C02 is the easiest to recognize because it presents the highest *posteriori* probability and classes C06,C09 and C10 present the lowest misclassification rate.

For the purpose of comparison, the texture identification experiments were also performed using traditional techniques such as Fourier descriptors [5, 1] and Gabor filters [4, 16, 10, 23]:

Fourier Descriptors: the Fourier descriptors for texture analysis consist of a feature vector with the energy of the most important N coefficients in the Fourier transform. In this case, N is the maximum radius allowed in the texture window, i.e., $N = 63$. As the low frequencies are found in the spectrum center (after shifting), each one of the coefficients corresponds to the sum of absolute values of a spectrum with a determined radial distance from the 2-dimensional transform center. Other Fourier

r_{max}	N^o of features	Average n^o of images correctly classified	Average success rate (%)	Standard deviation	Average max error (%)	Reliability
2	04	432.7	54.08	10.60	66.6	58.92
3	08	596.0	74.50	10.20	42.5	83.72
4	14	654.6	81.82	11.62	37.6	89.53
5	22	675.7	84.46	7.49	41.0	92.74
9	69	712.8	89.10	8.99	30.6	96.09
10	85	711.4	88.92	5.39	31.3	96.27
15	189	708.3	88.53	5.63	30.5	97.33
16	214	706.9	88.36	9.20	27.3	97.48
17	242	701.1	87.63	8.65	31.8	97.64
19	303	690.9	86.36	5.54	33.2	97.42
20	335	687.8	85.97	7.78	33.8	97.74

Table 3: Results for different r_{max}.

	C01	**C02**	**C03**	**C04**	**C05**	**C06**	**C07**	**C08**	**C09**	**C10**
C01	0.6625	0.025	0.025	0	0.0375	0.0375	0.0625	0.0375	0.025	0
C02	0	0.925	0	0	0	0	0	0	0	0
C03	0.025	0	0.925	0.0625	0	0	0	0	0.025	0
C04	0	0	0.0375	0.9125	0	0.0125	0	0	0	0
C05	0.05	0	0	0	0.925	0	0.025	0	0	0
C06	0	0	0	0	0	0.95	0	0	0	0
C07	0.05	0.025	0	0	0	0	0.8625	0.075	0	0.0125
C08	0.0875	0.0125	0	0	0.0375	0	0.05	0.8875	0	0
C09	0.05	0	0.0125	0.025	0	0	0	0	0.95	0.0375
C10	0.075	0.0125	0	0	0	0	0.005	0	0	0.95

Table 4: Confusion matrix for $r_{max} = 9$.

descriptors with orientation information are also used. 8 oriented sectors with 8 frequency bands obtaining 64 features ($N = 64$) were integrated. There are many alternative versions of this method in the literature, but in this paper only its two conventional implementations are considered (Fourier and Fourier Oriented);

Gabor Filters: a 2-D Gabor Filter is, basically, a bi-dimensional Gaussian function modulated by using a sinusoidal signal oriented in a determined frequency and direction. The procedure consists of the convolution of an input image by a Gabor filter family which presents various scales and orientations of an original configuration. The calculated energy for the obtained images consists of the feature set. Among the numerous tests performed, the best results were achieved using a family with 64 filters (8 rotations and 8 scales), with a lower frequency of 0.02 and an upper frequency of 0.5 (upper and lower frequencies are defined empirically). The setup of the individual parameters of each filter follows the mathematical model presented in [23, 33, 4].

Class	Reliability (%)
C01	91.32
C02	98.84
C03	97.34
C04	97.12
C05	96.15
C06	95.80
C07	93.86
C08	95.82
C09	97.86
C10	96.67

Table 5: Average reliability of all classes for $r_{max} = 9$

Table 6 summarizes the results presented by the evaluated techniques. Note that the proposed method is more robust for presenting the highest average sucess rate, lower standard deviation and the highest reliability, improving

Methods	N^o of features	Average n^o of images correctly classified	Average success rate (%)	Standard deviation	Average max error (%)	Reliability
proposed signature	69	712.8	89.10	8.99	30.60	96.09
Gabor	64	663.5	82.93	10.06	24.90	86.18
Fourier	63	666.3	83.28	13.22	34.90	80.16
Fourier Oriented	64	683.5	85.43	6.90	28.50	83.82

Table 6: Results yielded by the proposed method and traditional texture analysis techniques.

on traditional texture analysis methods. It is important to emphasize that these results consider $r_{max} = 9$. However, as previously shown, other values for r_{max} also yield good results.

6 Conclusion

We have presented a novel approach to extract morphometric characteristics from leaf textures for plant taxonomy applications. Both the effectiveness and efficiency of the method were demonstrated using various experiments. The method presented accuracy for the LDA rule as 89.60% and reliability as 97.12%, showing that the computed descriptors provide a good quality of discrimination rules. In addition, the system works properly for all tree classes considered. This characteristic shows the high method robustness.

Leaf texture identification is a difficult task because it often presents a high similarity of extra classes and a low similarity of intra classes. Although traditional texture analysis methods have provided satisfactory results, the volumetric Bouligand-Minkowski fractal dimension approach has proved to be superior for characterizing plant species. These results reinforce that this theory is efficient when it describes / characterizes events, phenomena and/or natural patterns such as plant leaves. Thus, leaf analysis and classification using volumetric fractal dimension is a valid and promising approach, and it can contribute significantly to other work of leaf identification already developed. Moreover, the method shows great potential in terms of being used as a feasible tool in many image analysis tasks, especially for applications involving biological images.

7 Acknowledgments

Odemir M. Bruno gratefully acknowledges the financial support of CNPq (National Council for Scientific and Technological Development, Brazil) (Grant #306628/2007-4) and FAPESP (The State of São Paulo Research Foundation) (Proc. #2006/54367-9 and #2006/53972-6). André R. Backes is grateful to FAPESP (Proc. #2006/54367-9) for his doctorate grant. Dalcimar Casanova is indebted to FAPESP (Proc. #2006/53972-6) for his master's grant.

References

[1] R. Azencott, J.-P. Wang, and L. Younes. Texture classification using windowed fourier filters. *IEEE Trans. Pattern Anal. Mach. Intell*, 19(2):148–153, 1997.

[2] R. K. Bajcsy. Computer identification of visual surfaces. *Computer Graphics Image Processing*, 2:118–130, Oct. 1973.

[3] V. Barnett and T. Lewis. *Outliers in statistical data*. Wiley, 1984.

[4] F. Bianconi and A. Fernández. Evaluation of the effects of gabor filter parameters on texture classification. *Pattern Recognition*, 40(12):3325–3335, 2007. URL `http://dx.doi.org/10.1016/j.patcog.2007.04.023`.

[5] R. N. Bracewell. *The Fourier Transform and Its Applications*. McGraw-Hill, New York, 3rd edition, 2000.

[6] O. M. Bruno, R. de O. Plotze, M. Falvo, and M. de Castro. Fractal dimension applied to plant identification. *Information Sciences*, 178:2722–2733, 2008.

[7] M. Carlin. Measuring the complexity of non-fractal shapes by a fractal method. *PRL: Pattern Recognition Letters*, 21(11): 1013–1017, 2000.

[8] Y. Q. Chen and G. Bi. On texture classification using fractal dimension. *IJPRAI*, 13(6):929–943, 1999.

[9] L. da F. Costa and R. M. C. Jr. *Shape Analysis and Classification: Theory and Practice*. CRC Press, 2000.

[10] J. Daugman and C. Downing. Gabor wavelets for statistical pattern recognition. In M. A. Arbib, editor, *The Handbook of Brain Theory and Neural Networks*, pages 414–419. MIT Press, Cambridge, Massachusetts, 1995.

[11] R. de O. Plotze, M. Falvo, J. G. Pádua, L. C. Bernacci, M. L. C. Vieira, G. C. X. Oliveira, and O. M. Bruno. Leaf shape analysis using the multiscale minkowski fractal dimension, a new morphometric method: a study with passiflora (passifloraceae). *Canadian Journal of Botany*, 83 (3):287–301, 2005.

[12] J. F. Hair, R. E. Anderson, R. L. Tatham, and Black. *Multivariate Data Analysis*. Prentice Hall College Div, 1998. Peter's book.

[13] R. M. Haralick. Statistical and structural approaches to texture. *Proc. IEEE*, 67(5): 786–804, 1979.

[14] L. R. Hickey. Classification of archictecture of dicotyledonous leaves. *Amer. J. Bot*, 60(1):17–33, 1973.

[15] P. W. Huang, S. K. Dai, and P. L. Lin. Texture image retrieval and image segmentation using composite sub-band gradient vectors. *J. Visual Communication and Image Representation*, 17(5): 947–957, 2006. URL `http://dx.doi.org/10.1016/j.jvcir.2005.08.005`.

[16] A. K. Jain and F. Farrokhnia. Unsupervised texture segmentation using Gabor filters. *Pattern Recognition*, 24(12):1167–1186, 1991.

[17] R. Johnson and D. Wichern. *Applied Multivariate Statistical Analysis*. Prentice-Hall, Englewood Cliffs, New Jersey, 1982.

[18] W. Judd, C. Campbell, E. A. Kellog, and P. Stevens. *Plant Systematics: A Phylogenetic Approach*. Sinauer Associates, Massachusetts, 1999.

[19] L. M. Kaplan. Extended fractal analysis for texture classification and segmentation. *IEEE Transactions on Image Processing*, 8(11):1572–1585, 1999.

[20] M. H. Kurmann and A. R. Hemsley. *The Evolution of Plant Architecture*. Royal Botanic Gardens, Kew, London, 1999.

[21] C. L. Lee and S. Y. Chen. Classification of leaf images. *International Journal of Imaging Systems and Technology*, 16(1): 15–23, 2006.

[22] J. Li, C. Sun, and Q. Du. A new box-counting method for estimation of image fractal dimension. In *International Conference on Image Processing*, pages 3029–3032, 2006. URL `http://dx.doi.org/10.1109/ICIP.2006.313005`.

[23] B. S. Manjunath and W.-Y. Ma. Texture features for browsing and retrieval of image data. *IEEE Trans. Pattern Anal. Mach. Intell*, 18(8):837–842, 1996.

[24] V. Murino, C. Ottonello, and S. Pagnan. Noisy texture classification: A higher-order statistics approach. *Pattern Recognition*, 31(4):383–393, 1998.

[25] X. Qiu and L. Wu. Nearest neighbor discriminant analysis. *IJPRAI*, 20(8):1245–1260, 2006. URL `http://dx.doi.org/10.1142/S0218001406005186`.

[26] M. Schroeder. *Fractals, Chaos, Power Laws: Minutes From an Infinite Paradise*. W. H. Freeman, 1996.

[27] A. Sengür, I. Türkoglu, and M. C. Ince. Wavelet packet neural networks for texture classification. *Expert Syst. Appl*, 32 (2):527–533, 2007.

[28] L. Shen and L. Bai. A review on gabor wavelets for face recognition. *Pattern Anal. Appl*, 9(2-3):273–292, 2006.

[29] C. Tricot. *Curves and Fractal Dimension*. Springer-Verlag, 1995.

[30] P. Tzionas, S. Papadakis, and D. Manolakis. Plant leaves classification based on morphological features and a fuzzy surface selection technique. In *5th Int. Conf. on Technology and Automation*, pages 365–370, Thessaloniki, Greece, 2005.

[31] M. Unser. Texture classification and segmentation using wavelet frames. *IEEE Trans. Image Processing*, 4(11):1549–1560, Nov. 1995.

[32] Z. Wang, Z. Chi, and D. D. Feng. Shape based leaf image retrieval. *IEE Proceedings-Vision Image and Signal Processing*, 150(1):34–43, Feb. 2003.

[33] E. Zhu, J. Yin, G. Zhang, and C. Hu. A gabor filter based fingerprint enhancement scheme using average frequency. *IJPRAI*, 20(3):417–430, 2006. URL `http://dx.doi.org/10.1142/S0218001406004740`.